Pitch and Yaw Control of Tailless Flapping Wing MAVs by Implementing Wing Root Angle Deflection

CHAN Woei Leong*, NGUYEN Quoc Viet, and Marco DEBIASI
National University of Singapore

ABSTRACT

Study was conducted on the effect of wing root angle deflection to pave the way for the implementation of tailless flight control on a hovering flapping wing platform. Hypotheses of how the wing root deflection in the sagittal direction could help generate pitching and yawing moments are presented and investigated. The investigation was completed using a four bar linkage crank-rocker flapping mechanism. The flapping frequencies are from 13Hz to 18Hz, and the sagittal deflection angle ranged between -6.7° to 7°. Study shows that tailless pitch and yaw control is feasible but the nonlinearities could lead to huge challenge on implementation. The deflection angle also compromises lift.

1 INTRODUCTION

Flapping wing micro air vehicle (FW-MAV) has been around for quite some time. Earlier flapping wing MAVs such as the DelFly [1] employs tail control. Pitch, and yaw moments are generated by conventional control surfaces like the fixed wing aircraft. In the latest edition of the DelFly, the DelFly Explorer [2] has a pair of ailerons for roll control. Due to biomimicry reason, tailless control has gained a lot of interests recently. Unlike birds, insects fly without using tail; the only way to manoeuvre is by changing the wing kinematics. Dickinson [3] argued that the rotational force plays an important part in insect flight control and the insects regulates rotational phase for flight manoeuvres. Dickinson also explained explicitly how the insects perform flight control about the three rotational axes [4]: mean stroke position is altered to generate pitch moment; yaw is achieved by differential adjustment of stroke amplitude; roll is achieved by differential inclining of the stroke planes of the wings.

The first successful implementation of tailless control on a standalone artificial platform was demonstrated by Keennon [5] on the Nano Hummingbird. The Nano Hummingbird uses a combined wing twist and rotation modulation to achieve flight control. The other iconic standalone flapping wing platforms that utilize tailless control are the Techjets Dragonfly [6], and the FESTO BionicOpter [7]. The smallest, but not standalone tailless flapping wing platform is the Robobee [8, 9]. Other than that, Phan *et al.* [10] designed a flapping mechanism that can generate pitching moment by changing the stroke angle range, a mechanism similar to the real insect, Oppenheimer *et al.* [11] studied the utilization of split-cycle constant-period frequency modulation for flapping wing flight control, and Hale *et al.* [12] tried to do so by varying wing membrane stiffness.

The Temasek Laboratories of the National University of Singapore has started developing flapping wing MAVs since two years ago. Insect inspired prototypes are built and flight tested. A four-winged and a two-winged hovering flapping wing platform with tail control was developed. However, the flight quality of the two-winged platform is deficient due to unsound flight control and stability. The present work is focused on studying the effect of deflecting the wing root in the sagittal direction (forward and backward). We hypothesized that the deflection will result in changes of pitching and yawing moments. Understanding the effect of moment changes will help pave the way of utilizing the effect for flight control in future tailless flapping wing platform. Section 2 of this paper explains the hypotheses of pitch and yaw moment generation by deflecting the wing root. The flapping mechanism and the wing, and the experimental setup are being elaborated in Section 3 and 4 respectively. Force and moment measurements are presented and discussed in Section 5. Finally, the conclusions end the paper.

2 HYPOTHESES

Figure 1 illustrates the right wing deformation during a downstroke at positive deflection angle. Deflection to the front (ventral) is defined as positive. The angle is parallel to the sagittal plane, thus called sagittal deflection angle ($\delta_{s,r}$).

2.1 Pitching Moment

It is defined in this paper that a ventral-stroke is when the leading edges of the wings are at the ventral side of the flapping wing platform. The end of downstroke and the beginning of upstroke (supination) occurs during the ventral-stroke. Similarly, the dorsal-stroke is when the leading edges of the wings are at the dorsal side.

At a positive sagittal deflection angle, the wing is slacker at the ventral-stroke. We hypothesized that a slacker wing would allow more wing rotation, and more lift to be generated. Likewise, a stretched wing at the dorsal-stroke discourages wing rotation and produces less lift. The lift difference results in an unbalanced pitching moment. A positive sagittal

*Email address(es): tslcwl@nus.edu.sg

deflection angle on either right or left wing will result in a pitch up moment as illustrated in Figure 1.

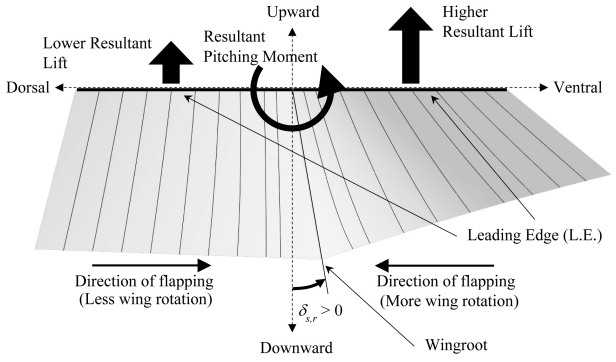

Figure 1: Pitching moment generated due to wing root deflection viewed from right side.

2.2 Yawing Moment

At a positive sagittal deflection angle, the right wing is rotated more during the upstroke, thus reducing drag. The same phenomenon happens when the left wing has a negative sagittal deflection angle during downstroke. We hypothesized that the drag difference between the down and upstrokes creates an unbalanced yawing moment. A positive and negative sagittal deflection angles on the right and left wings respectively will result in a positive yawing moment as illustrated in Figure 2.

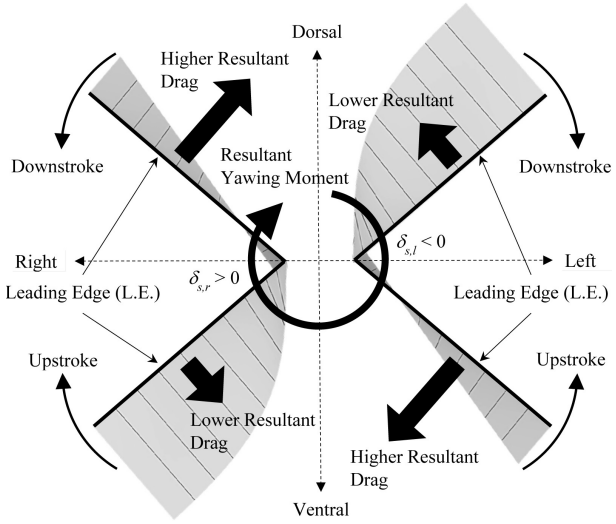

Figure 2: Yawing moment generated due to wing root deflection.

3 Flapping Mechanism and Wing

3.1 Flapping Mechanism

The flapping mechanism being used in the experiment is a four bar linkage crank-rocker system as shown in Figure 3. The gearbox structural components were cut out of a 1mm thickness glass epoxy panel using a CNC milling machine. The gears are off-the-shelf Nylon gears and brass pinion with a total gear ratio of 16:1. OverSky HP03S 16600kV brushless motor was used to drive the mechanism. The stroke angle (ϕ) range is $\pm 64°$. Critical dimensions of the gearbox are l_0 = 12.6mm, l_1 = 4.5mm, l_2 = 12.5mm, and l_3 = 5.0mm. Doman *et al.* [13] has derived mathematical models for a four bar linkage mechanism. The models are presented here as Equation 1 to 4. Equation 5 represents the relation of the rocker output angle (ϕ_l) to the stroke angle (ϕ) of the flapping mechanism presented in this paper.

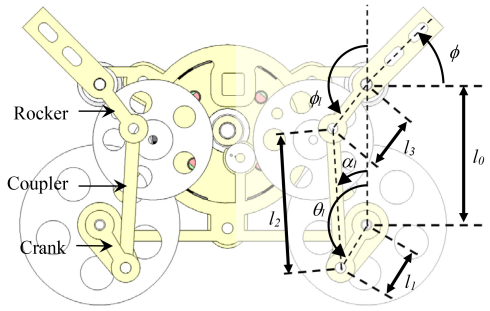

Figure 3: Four bar linkage crank-rocker flapping mechanism.

$$\alpha_l = \arctan 2\left(\frac{l_3 \sin\phi_l - l_1 \sin\theta_l}{l_0 + l_3 \cos\phi_l - l_1 \cos\theta_l}\right) \tag{1}$$

$$\phi_l = 2 \cdot \arctan 2\left(\frac{-K_1 \pm \sqrt{{K_1}^2 - {K_3}^2 + {K_2}^2}}{K_3 - K_2}\right) \tag{2}$$

where $K_1 = -2l_1 l_3 \sin\theta_l$
$K_2 = 2l_3(l_0 - l_1 \cos\theta_l)$
$K_3 = {l_0}^2 + {l_1}^2 - {l_2}^2 + {l_3}^2 - 2l_0 l_1 \cos\theta_l$

$$\dot{\alpha}_l = \frac{l_1 \sin(\phi_l - \theta_l)}{l_2 \sin(\alpha_l - \phi_l)}\dot{\theta}_l \tag{3}$$

$$\dot{\phi}_l = \frac{l_1 \sin(\alpha_l - \theta_l)}{l_3 \sin(\alpha_l - \phi_l)}\dot{\theta}_l \tag{4}$$

$$\phi = \phi_l - 97.63° \tag{5}$$

Assumed that the crank angle (θ_l) varies at constant angular rate, Figure 4 shows the ideal stroke angle within one flapping cycle under no load condition calculated using Equation 5. It shows that the downstroke and upstroke are not symmetrical. The angular rate of upstroke is generally constant, but the downstroke starts at a lower angular rate and accelerates throughout the stroke. The duration of upstroke is fractionally longer than the downstroke.

Assumed there is no power loss throughout the crank-rocker, one is able to calculate the ratio of output torque to input torque using Equation 6. Figure 5 shows the torque ratio throughout the strokes. Apparently the torque ratio at

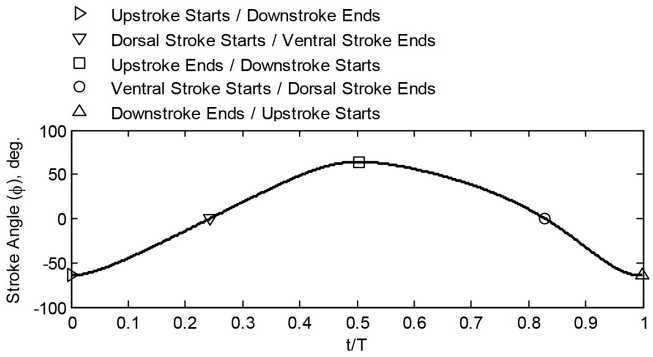

Figure 4: Ideal stroke angle without load.

the beginning of downstroke is significantly higher and reduces throughout the half stroke, while torque ratio variation of upstroke is relatively flat. It suggests that under loaded condition, the stroke angle changes rapidly at the beginning of downstroke, possibly produce higher lift as compared to the upstroke. The average torque ratio of downstroke is also higher than the upstroke. Since the stroke angle ranges of downstroke and upstroke are symmetrical, it suggests that under loaded condition, the duration of downstroke is shorter. Similarly, the duration of dorsal-stroke is supposedly shorter.

$$\frac{\tau_0}{\tau_i} = \frac{l_3 \sin(\alpha_l - \phi_l)}{l_1 \sin(\alpha_l - \theta_l)} \tag{6}$$

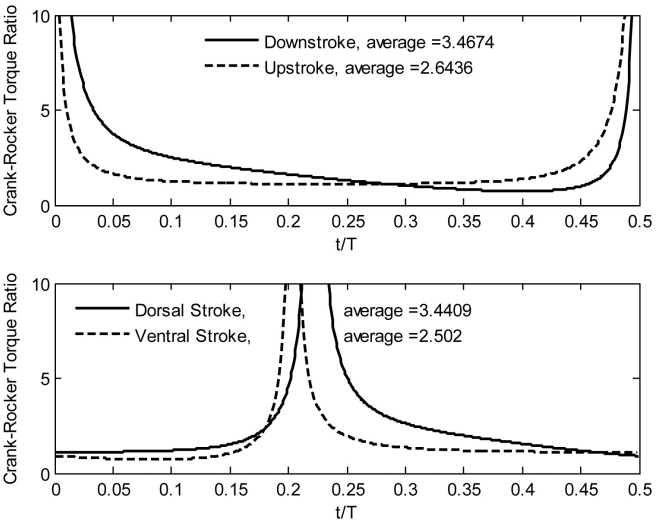

Figure 5: Flapping mechanism crank-rocker torque ratio.

3.2 Wing

Figure 6 shows a drawing of the wing used for the experiment. The wing is in rectangular shape of which the half wingspan is 90mm and the chord length is 50mm. At the wing root, there is a 10° of slack angle. The wing root and leading edge are perpendicular to each other after installation onto the flapping mechanism. Figure 7 and 8 show the wing being attached on the experimental setup. As shown in the figures, the wing root slack angle allows the wing to have limited rotation about the leading edge and encourages wing rotation during flapping.

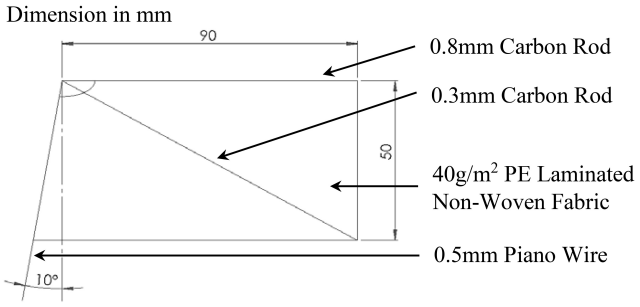

Figure 6: Wing dimension and materials.

The wing membrane is 40g/m2 polyethylene (PE) laminated non-woven fabric. Non-woven fabric was chosen instead of the more frequently used Mylar because it can easily adhere to adhesives and it produces lesser acoustic signal. Non-woven fabric is porous, and porosity reduces lift. Due to that, it is required to have a layer of PE lamination. As illustrated in Figure 6, the leading edge of the wing is a 0.8mm carbon rod, the wing root is 0.5mm piano wire, and the wing stiffener is made out of 0.3mm carbon rod. The total weight of one wing is 0.6g.

4 Experimental Setup

A test fixture as shown in Figure 7 is specifically designed and fabricated for the experiment. The test fixture accommodates the flapping mechanism. The wing holder holds the leading edge of the wing and the bottom end of the wing root is secured on a rotatable arm. The fixture allows adjustment of the wing sagittal deflection angle by securing the rotatable arm on the fixture through different threaded holes. It also allows the adjustment of coronal deflection, but the effect of coronal deflection will not be discussed in this paper.

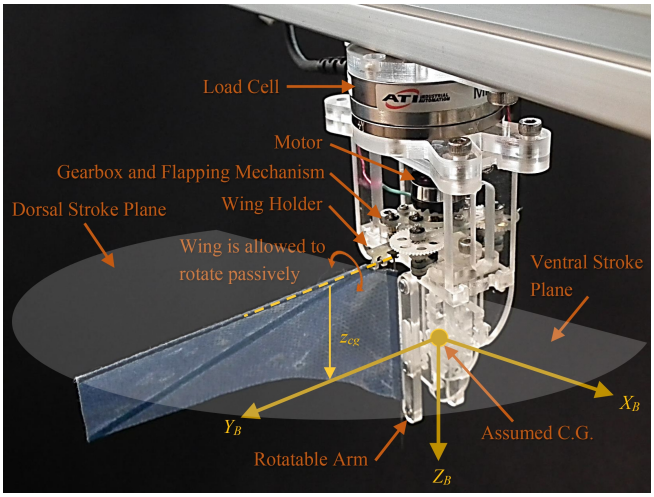

Figure 7: Experimental setup.

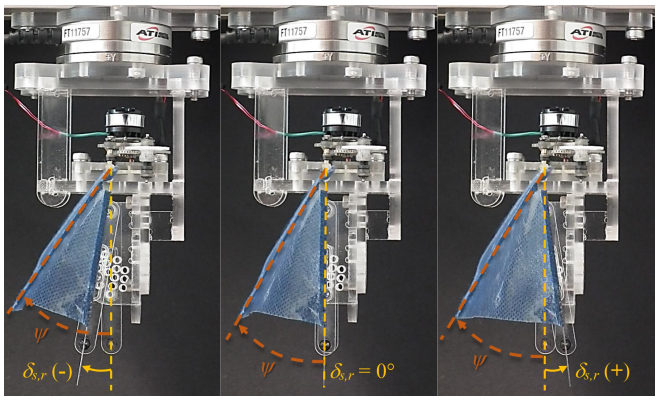

Figure 8: Side view of experimental setup showing the sagittal deflection angle of the right wing.

A load cell (ATI Mini40) is installed on top of the test fixture, and the load cell is fixed on a beam. The load cell measures 3-axis forces and 3-axis moments at a sampling rate of 5000Hz. The measured data was then transformed to the body-fixed coordinate system about the assumed centre of gravity (CG) of the eventual flying platform using Equation 7. The assumed CG is the intended centre point of the flying platform rotational motion. The distance of the assumed CG from the leading edge is being designated as z_{cg}. The origin of the body-fixed coordinate system is the assumed CG, X_B-axis points forward, Y_B-axis points to the right side, and Z_B-axis points downward. F_x, F_y, F_z, and M_x, M_y, M_z, are forces and moments about the X_B, Y_B, and Z_B-axis respectively.

$$M_{y,z_{cg}} = M_{y,z_{cg}=0} - F_x z_{cg} \tag{7}$$

where $M_{y,z_{cg}=0}$ is the pitching moment at $z_{cg} = 0$

Only the right wing is used for the experiment in order to better study the effect of the deflection. If needed, the effect of two wings can be easily deduced from the single wing data by assuming that the two wings are identical using $F_{x,l} = F_{x,r}$, $F_{y,l} = -F_{y,r}$, $F_{z,l} = F_{z,r}$, $M_{x,l} = -M_{x,r}$, $M_{y,l} = M_{y,r}$, and $M_{z,l} = -M_{z,r}$, where subscripted r and l represents right and left wing respectively. The data presented in this paper is of single wing (right wing) measurement unless mentioned otherwise.

The wing is allowed to rotate passively about the wing holder. Figure 8 shows the right view of the experimental setup with sagittal deflection angle of the right wing. From the figure, one can conceive that the wing will be slacker throughout the ventral stroke at a positive sagittal deflection angle as described earlier. A slacker wing allows more rotational angle (ψ) during the flapping motion. Similarly, a negative sagittal deflection angle encourages larger wing rotation at the dorsal-stroke.

Tests were conducted from 13 to 18Hz flapping frequency, the sagittal deflection angle ranged between -6.7° to 7°, and without incoming flow to simulate hovering condition. Given the kinematics viscosity of $1.57 \times 10^{-5} m^2 s^{-1}$, the equivalent Reynolds number as defined by Shyy *et al.* [14] is in between 16637 to 23036. The force and moment data presented in the paper are not pure aerodynamic force, they are the sum of aerodynamic and inertia forces, thus the data are not made dimensionless.

5 Results and Discussion

5.1 Forward Force (F_x)

Figure 9 shows the variation of forward force (F_x) in one flapping cycle and the corresponding stroke angle. The stroke angle was captured from the images taken by a PCO 1600 sensitive camera. The horizontal axis of the figure is time being normalized to the flapping cycle period. The force data is an average of 18 repeated flapping cycles. The error bar shows that the force measurement is repeatable. Likewise, all other data of force and moment variations in a flapping cycle shown in the paper are the result of averaging the measurement of multiple cycles at their corresponding flapping frequency and sagittal deflection angle. Forward force is dominated by inertia force and as shown in the figure, it reaches the minimum at the beginning of downstroke (supination). All data of force and moment variations in a flapping cycle shown in the paper are arranged such that they start at the point of minimum forward force which presumably the point of supination. The wing kinematics wasn't monitored for all cases due to hardware limitation.

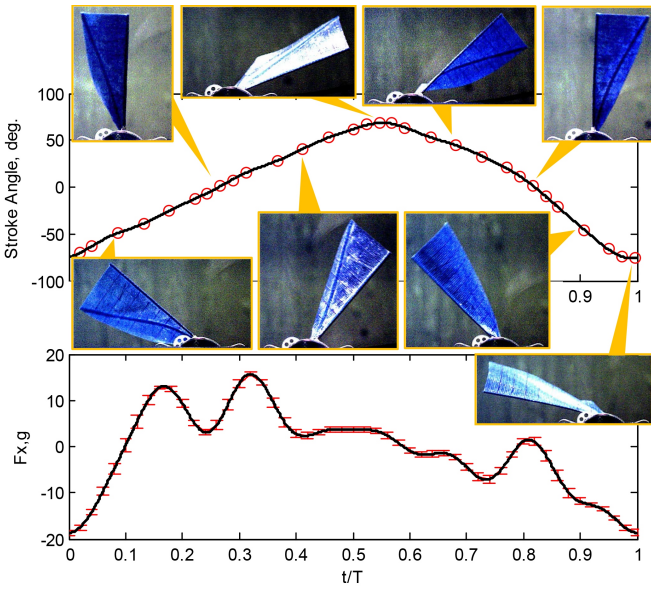

Figure 9: Stroke angle and corresponding forward force (wings as seen from the top).

Figure 10 shows the forward force variations in a flapping cycle at various flapping frequencies and sagittal deflection angles. The data starts at the beginning of upstroke, which corresponds to the minimum. It follows by two posi-

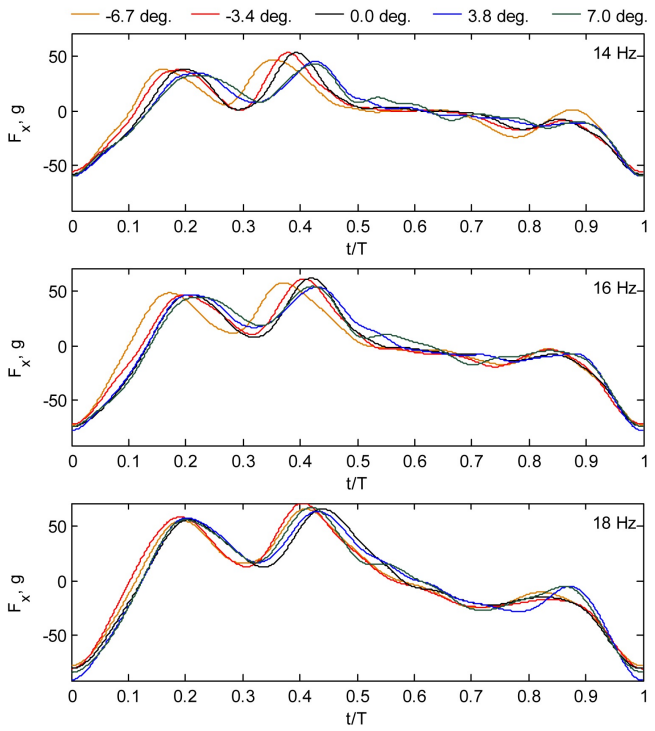

Figure 10: Forward force in one flapping cycle.

tive peaks. The figure shows that the more positive the sagittal deflection angle is, the later the peaks tend to occur. From Figure 9, the peaks occur during the first half of the downstroke when the wing is still in the ventral side. The delay could be due to the fact that the more positive the sagittal deflection angle is, the slacker the wing is at the ventral side

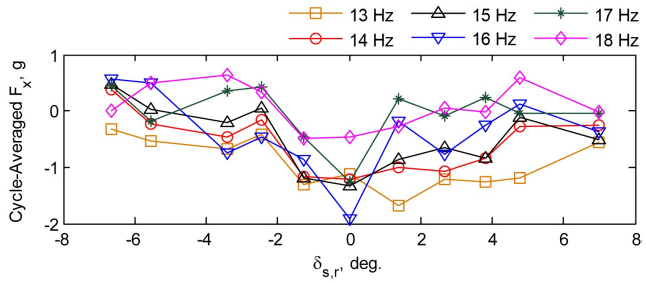

(a) Measurement

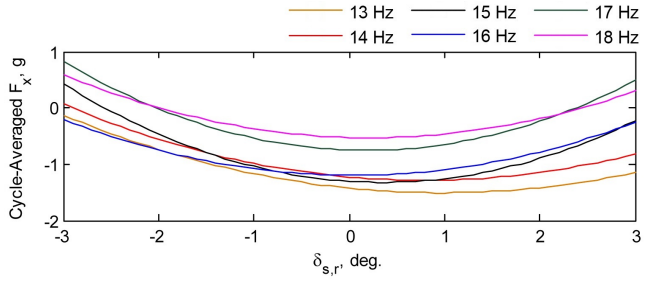

(b) Quadratic regression

Figure 11: Cycle-averaged forward force.

and thus it takes longer to be fully rotated. However, as the flapping frequency increases, this phenomenon subsides.

Figure 11 shows the cycle-averaged forward force ($\bar{F}_x$). At zero sagittal deflection angle, the cycle-averaged forward force is negative, but the magnitude is less than 2g. As the sagittal deflection angle moves away towards either the positive or negative direction, the magnitude of cycle-averaged forward force tends to decrease. The cycle-averaged forward force is in the range of -2g to 1g, it should not have significant effect on the translational motion, but it has significant impact on the pitching moment as discussed later. Figure 11(b) shows the result of quadratic regression of the cycle-averaged forward force within a smaller range of the sagittal deflection angle. Apparently, the cycle-averaged forward force is at its maximum magnitude at 0° to 1° sagittal deflection angle.

5.2 *Lift Force (L)*

The lift force ($L = -F_z$) is being presented in Figure 12. There are peaks of lift force right after the start and at the middle of the upstroke. We will refer to the peaks as the first and second peak respectively. The first peak reduces and the second peak increases as the sagittal deflection angle increases. The first peak occurs after supination, thus its reduction with sagittal deflection angle suggests that the slacker wing do not guarantee higher lift generation after all. Also observed is the delay of the second peak as the sagittal deflection angle increases. Negative peaks are also present right before the positive peaks, and the magnitude of the negative peaks increases as the corresponding positive peaks increases.

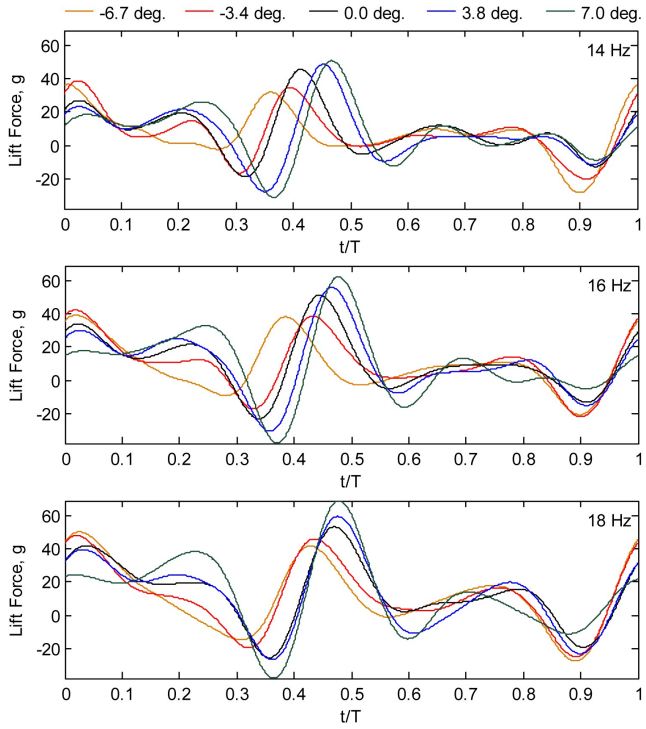

Figure 12: Lift force in one flapping cycle.

As the flapping frequency increases, the magnitude of the positive peaks increases, but the magnitudes of the negative peaks do not increase significantly, resulting in an increase of total lift as shown in Figure 13. Figure 13 shows that the magnitudes of the cycle-averaged lift ($\bar{L} = -\bar{F}_z$) are at the maxima when the wing root is not deflected, indicating that tailless control compromises lift.

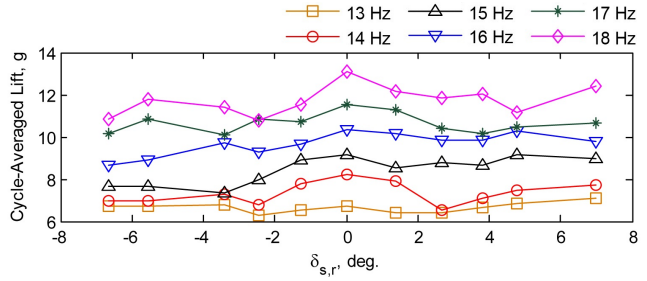

(a) Measurement

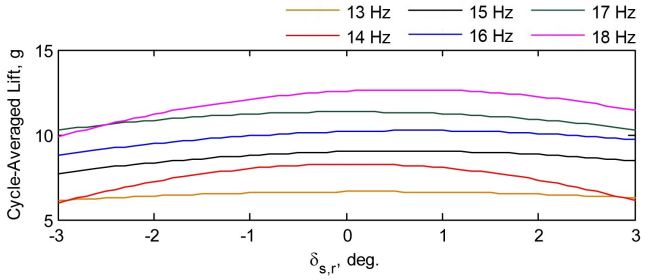

(b) Quadratic regression

Figure 13: Cycle-averaged lift.

5.3 *Pitching Moment (M_y)*

Figure 14 clearly shows the pitching moment is more closely correlated to the forward force than the lift. Evidently, the pitching moment hypothesis is over simplified. Figure 15 shows the pitching moment variation at 18Hz at six difference CG locations, namely half chord distance above the stroke plane (z_{cg}=-25mm), the stroke plane (z_{cg}= 0mm), half chord below (z_{cg}=25mm), and one chord below (z_{cg}=50mm) the stroke plane respectively. As shown in the figure, the further away the CG from the half chord below stroke plane (z_{cg}=25mm) in either directions, the pitching moment become more correlated to the forward force. This is due to the distance of the CG and the acting point of forward force. The distance is the moment arm, and the pitching moment is dominated by the forward force when the length of moment arm is significant. One must not confused this forward force acting point with the centre of pressure because the forces measured are the sum of aerodynamic force and inertia force. From the observation, it can be safely inferred that the average vertical coordinate of the forward force acting point is at the half chord below the stroke plane (z_{cg}=25mm).

As shown in Figure 16, as the CG being shifted downward, the cycle-averaged pitching moments ($\bar{M}_y$) tend to have double troughs patterns with the centre peaks at zero

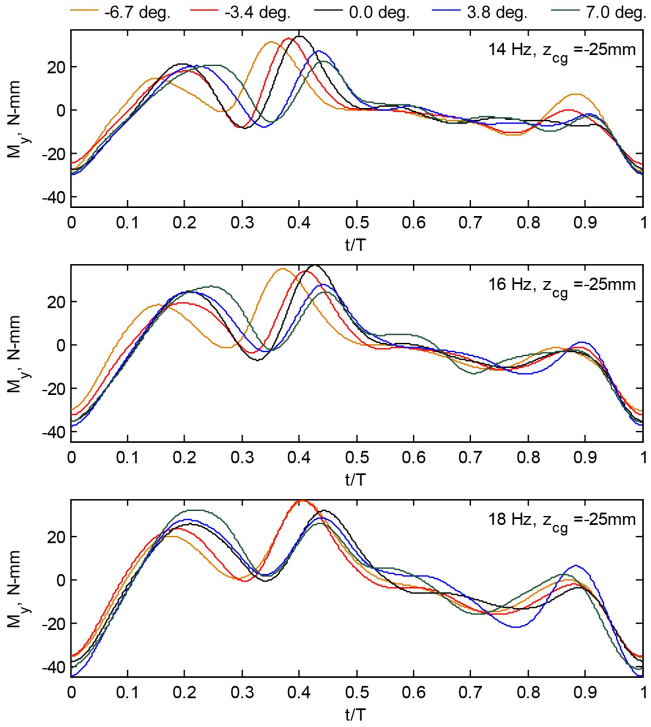

Figure 14: Pitching moment in one flapping cycle.

sagittal deflection angle. The magnitude also tend to increase and eventually the cycle-averaged pitching moments of the lower flapping frequencies (13Hz to 16Hz) only distribute in the positive region and pitch control in these frequencies are deemed infeasible.

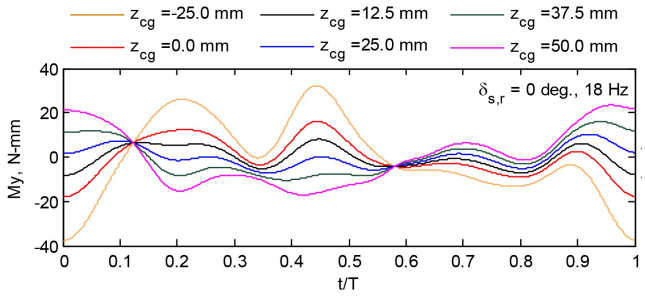

Figure 15: Pitching moment about various CG locations in one flapping cycle ($\delta_{s,r} = 0°$ at 18Hz).

In summary, in order to have better pitch control characteristics and flight stability, the option is to have the CG located at half chord and flap at higher frequency. Flapping at higher frequency ensures that the cycle-averaged pitching moment is being distributed in both positive and negative regions. However, the double troughs nonlinearity will still bring about huge challenge in pitch control implementation.

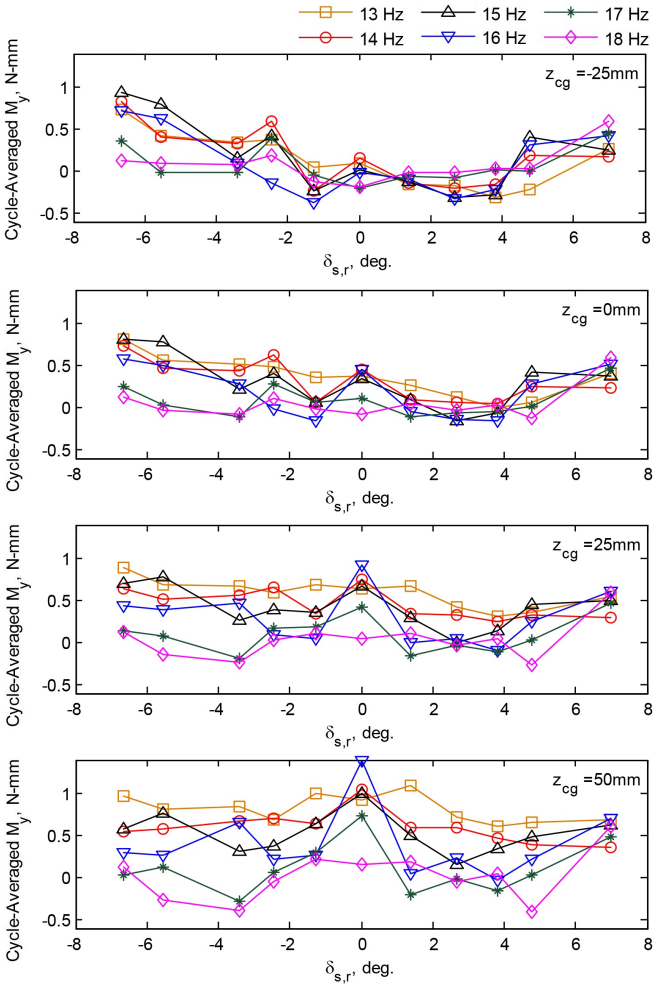

Figure 16: Cycle-averaged pitching moment.

5.4 *Yawing Moment (M_z)*

Assumed that the flying platform is symmetrical about the X_B-Z_B-plane, then the yawing moment is not affected by the shifting of CG along Z_B-axis. The two contributors to the yawing moment are the forward and sideward force. Figure 17 shows the variation of the yawing moment with a flapping cycle at different sagittal deflection angles for three different flapping frequencies. Similar to the pitching moment hypothesis, the yawing moment hypothesis seems to be over simplified. Instead of generating positive and negative yawing moments throughout the whole downstroke and upstroke respectively, positive and negative yawing moments are generated roughly during the dorsal-stroke and the ventral-stroke respectively. Yawing moment due to the motor rotation is assumed to be negligible because the moment is so small that the load cell is unable to measure it.

The cycle-averaged yawing moments are presented in Figure 18. In general, the yawing moments have positive slope in the negative sagittal deflection angle region and a milder negative slope in the positive sagittal deflection angle region. The cycle-averaged yawing moment is almost always

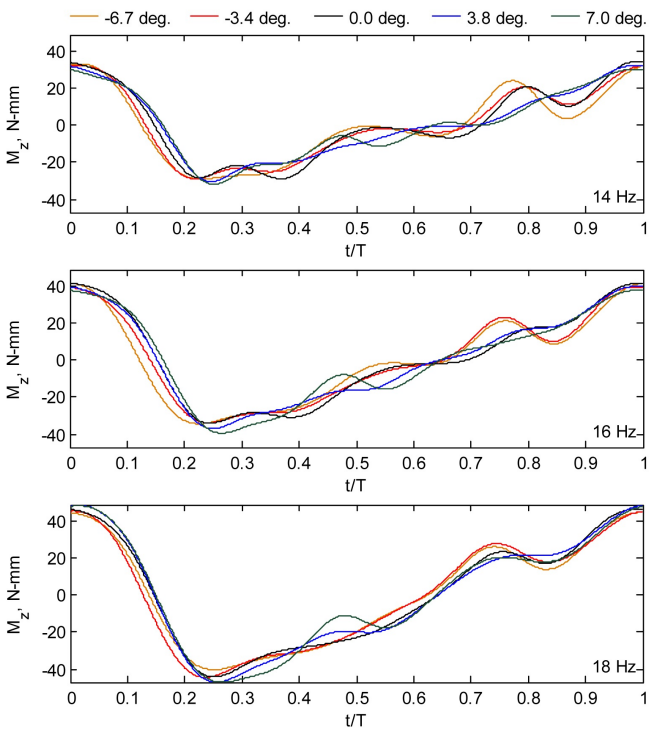

Figure 17: Yawing moment in one flapping cycle.

positive, contrary to what was hypothesized. However, yawing control is still implementable if the effect of the left wing is taken into account.

Figure 19 shows how the total cycle-averaged yawing moment ($M_{z,T}$) at 16Hz flapping frequency is being shifted vertically if an identical left wing is being deflected. The data

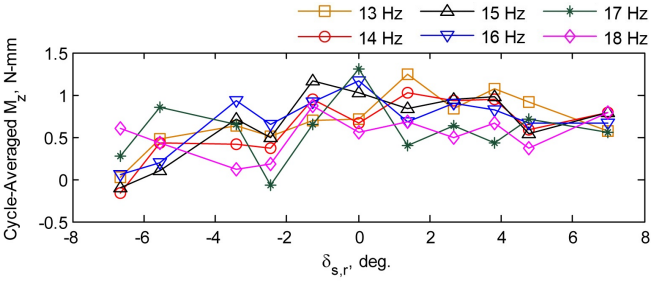

(a) Measurement

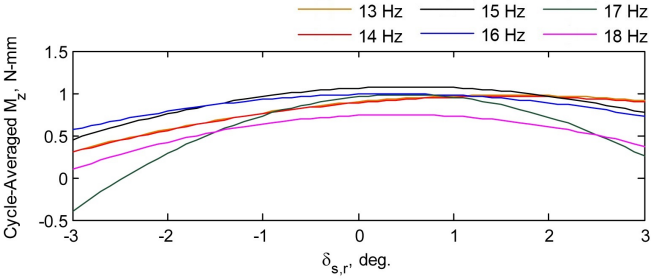

(b) Quadratic regression

Figure 18: Cycle-averaged yawing moment.

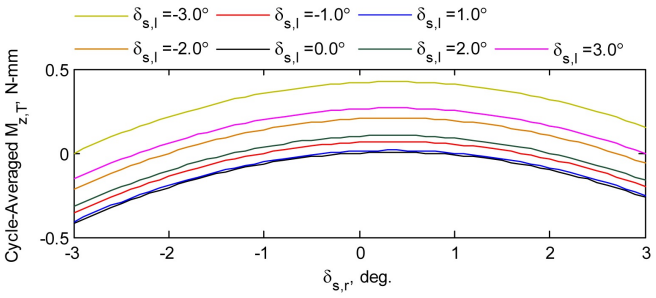

Figure 19: Total yawing moment with difference sagittal deflection angles at both wings (16Hz).

is deduced from the quadratic regression of the single wing measurement. By using different combinations of the left and right wing sagittal deflection angles, positive and negative yawing moments can be generated. Thus yawing control is possible albeit the challenge due to the nonlinearity.

6 Conclusion

The effect of deflecting the wing root in the sagittal direction and the possibility of using the effect for pitch and yaw control are investigated. The flapping mechanism is a four bar linkage crank-rocker system which has unsymmetrical stroke angles and torque output. The hypotheses are proven to be over simplified. A more thorough study must be conducted in order to fully understand the physical phenomena when the sagittal deflection angle is applied, such to better capitalize the effect in future designs.

It is discovered that the best CG location is at the half chord distance below the stroke plane. It is possible to implement the sagittal deflection angle for flight control, but it is a huge challenge due to the nonlinearities. Furthermore, pitch and yaw are coupled, and it is quite a challenge to find an equilibrium point where by the total sums of the moments and forces are zeroes. Apart from the pitching and yawing moments, sagittal deflection angle delays the force peaks. This effect subsides as the flapping frequency increases. Lastly, the deflection also compromises lift.

Future study could be including designing a symmetrical stroke mechanism such that the forces and moments are at equilibrium when the wings are not deflected, and conducting studies with other wing materials and configurations at higher flapping frequencies. Wing kinematics capture and flow visualization are also essential in order to have better understanding on the force and moment variations. Higher resolution on the deflection angle is also very important to capture the cycle-averaged force and moment variations accurately. Study will also be conducted to investigate the effect of wing root deflection in the coronal direction.

Acknowledgements

Authors appreciate the financial support from Future System and Technology Directorate of Singapore (Programme No. PA 9011102539).

References

[1] M. Groen, B. Bruggeman, B. Remes, R. Ruijsink, B. van Oudheusden, and H. Bijl. Improving flight performance of the flapping wing MAV DelFly II. In *International Micro Air Vehicle conference and competitions (IMAV)*, 2010.

[2] TU Delft's Delfly Explorer, available at http://www.delfly.nl/explorer.html

[3] M.H. Dickinson, F. Lehmann, and S.P. Sane. Wing rotation and the aerodynamic basis of insect flight. *Science*, 284 (5422): 1954-1960, 1999.

[4] W.B. Dickson, A.D. Straw, C. Poelma, and M.H. Dickinson. An integrative model of insect flight control. In *AIAA Aerospace Sciences Meeting and Exhibit*, 2006.

[5] M. Keennon, K. Klingebiel, H. Won, and A. Andriukov. Development of the Nano Hummingbird: a tailless flapping wing micro air vehicle. In *50th AIAA Aerospace Sciences Meeting*, 2012.

[6] Techjet's Dragonfly, available at http://www.techject.com/

[7] Festo's BionicOpter, available at http://www.festo.com/

[8] R.J. Wood. Design, fabrication, and analysis of a 3 DOF, 3cm flapping-wing MAV. In *IEEE/RSJ International Conference on Intelligent Robots and Systems (IROS)*, 2007.

[9] K.Y. Ma, P. Chirarattananon, S.B. Fuller, R.J. Wood. Controlled flight of a biologically inspired, insect-scale robot. *Science*, 340 (6132): 603-607, 2013.

[10] V.H. Phan, T.Q. Truong, and H.C. Park. Pitching moment generation for longitudinal attitude control of insect-mimicking flapping wing system. In *10th International Conference on Ubiquitous Robots and Ambient Intelligence (URAI)*, 2013.

[11] M.W. Oppenheimer, D.O. Sigthorsson, I.E. Weintraub, D.B. Doman, and B. Perseghetti. Wing velocity control system for testing body motion control methods for flapping wing MAVs. In *51st AIAA Aerospace Science Meeting*, 2013.

[12] L. Hale, M. Patil, and C. Woolsey. Control of flapping wing MAV using variable stiffness membrane wings. In *51st American Control Conference*, 2012.

[13] D.B. Doman, C.P. Tang, and S. Regisford. Modeling interactions between flexible flapping wing spars, mechanisms, and drive motors. *Journal of Guidance, Control, and Dynamics*, 34(5): 1457-1473, 2011.

[14] W. Shyy, Y. Lian, J. Tang, D. Viieru, and H. Liu *Aerodynamics of low Reynolds number flyer*. Cambridge University Press, New York, 2008.